

On the adhesion features of Ag nanolayers on differently-passivated Si(001)(2x1) substrates

A. IOANID*, M. DIEACONU, S. ANTOHE

Faculty of Physics, University of Bucharest, Bucharest-Magurele, Romania

Modelling of the metallic overlayer properties demands the understanding of the physical features of the metal/support adhesion that is possible by a quantitative analysis of the intim metal-atom/support-atom interactions. We propose an quantitative evaluation for the silver (Ag) structures deposited on porous silicon(PS) surface, that is of the interactions Ag^0/PS and Ag^+/PS at PS/aqueous AgNO_3 solution interface, for three types of terminated PS surface, Si-H, Si-O, Si-OH. Mainly results show that the binding energy metal/support, is greatest for hydrophilic surface support (Si-O and Si-OH) for both metal atoms and ions and that the metal structures (few atomic layer thickness) deposited on hydrophilic surface consists mainly from islands, while that deposited on hydrophobic surface are rather compact films.

(Received August 18, 2011; accepted November 23, 2011)

Keywords: Pair potential, N-body potential, Dispersive interaction, Surface polarity, Lateral diffusion

1. Introduction

The knowledge of the adhesion mechanism of the noble metals on semiconductor surface is the main problem for modelling the metallic overlayer properties. The understanding of the growth of the metal thin film is very important both from fundamental and practical viewpoint. The physical properties depending both on the morphology and structure of the layer, particulary the noble metal/semiconductor nanostructures lead to interesting applications in the fields of catalysis, biosensing, electronics and optics.

The integration of nanomaterials with these crucial domains has leads to the development of diagnostic devices, contrast agents, analytical tools, implantable sensors to recognize disease processes in their early stages, physical therapy applications, drug delivery vehicles.

Antibacterial properties of Ag coupled to those of biocompatibility of porous silicon on one part, and the size of nanometerials similar to that of most biological molecules and structures , on the other hand, make using for both in vivo and in vitro biomedical research and applications. Silver has for a long time been known to be toxic to a wide range of bacteria (e.g., *E. coli*), and this has been utilized in various applications. Silver compounds are used as preservatives in a variety of products and in the medical field to treat burns and infections. The bactericidal effect of silver has two components: one reactive being either silver ions or silver nanoparticles and one of trans-membrane and intra-cell transport. Experiment have shown that silver nanoparticles exhibit bactericidal properties and that these effects depend strongly upon the size and shape of the nanoparticles [1].

All the applications using these metallic nanostructures exploit their abbility to selectively recognize the guest species via a macroscopic physical response. For the noble

metal nanostructures it is possible due to their intensive surface plasma resonance (SPR) in the ultraviolet-visible (UV-VIS) and near infrared (NIR) of electromagnetic wavelength. Silver nanostructures exhibit intensive SPR band in the wavelenght range $200 \div 900\text{nm}$. To date, one very important optical application of silver nanostructures is the study of the vibrational signature of an solute molecule using surface enhancement Raman scattering (SERS) measurements [2].

The Ag film morphology depends both on deposition conditions and on structural and compositional properties of Si surface. It is found that Ag grows epitaxially on both Si(001) and Si(111) through coincident site lattice matching though there is a large, 25%, lattice mismatch [3]. The features of the growth of thin and ultrathin Ag films on hydrogen-terminated Si(111) has been investigated *in situ* by electrical resistance measurements and by *ex situ* AFM characterization. The films were deposited by electron beam evaporation at a rate of 0.01nm/s under ultrahigh vacuum conditions and at substrate temperature from $130 \div 550\text{K}$. The electrical resistivity drops (decreases abruptly) for thickness of film above 5nm . The large electrical rezistivity from very thick films can be associated with an supplementary scattering effect of the conduction electrons due to surface roughness, implies that for ultrathin films the increase is still more rapid and thought to be associated with discontinuities and island formation [4].

The Ag films with controlable morphology and sizes may be obtained by the simple electroless metal-deposition method. Thus, immersing a cleaned silicon wafer into an aqueous solution of AgNO_3 and ammonia fluoride, in [5], has been simultaneously prepared well-defined silver dendrites and thin porous silicon layers. By lateral diffusion mechanism is possible a continuous aggregation growth of silver dendritic nanostructures on a

layer of silver nanoislands or nanoclusters (Volmer-Weber layer). The SERS effect of this silver dendritic layer permits Raman analysis of Rhodamine B molecule from $10^{-5} M$ aqueous solution [5]. Due to long range lateral diffusion of Ag atoms, the effective metal thickness deposited by epitaxy, is of monolayer range (1ML). Also, the lateral mobility of Ag atoms on H-terminated Si (100) is high and sufficient for a lateral self-assembly of a complete atomic layer. Usually, the self-assembly occurs either at early stages of Stranski-Krastanov epitaxial growth [6] (wetting layer) or during layer-by-layer epitaxial growth [7]. The first step of the deposition metallic film process consists to the interactions between metal and substrate surface atoms. These interactions depend on nature implying atoms, on substrate surface polarity and may lead to simply adhesion by physisorption (non-bonding) or to a strong adhesion by chemisorption (bonding) corresponding to any hydrophobic/hydrophilic (dewetting/wetting) properties of the substrate/solvent interface. Both, substrate atoms nature and substrate surface polarity depend on passivation/functionalization of free surface of semiconductor. The growth and dynamic of the active noble metal as adsorbate depends on the polar/nonpolar properties of the substrate surface.

The aim of this work is an analysis of the physical features of the Ag as noble metal adhesion on porous silicon (PS) surface by a quantitative evaluation of the

interactions Ag^0/PS and Ag^+/PS at PS/aqueous AgNO_3 solution interface, for three types of terminated PS surface, Si-H, Si-O, Si-OH. Our analysis for the Ag/PS interface interactions considers the pair interatomic potentials with repulsive, dispersive and electrostatic terms for the Ag/PS interactions and the Gupta energetic model for Ag/Ag interactions. Parameters for used potentials are mainly empirical fitting experimental results and partially from ab initio evaluation (e.g., ionization potential as cluster's model computing).

2. Modelling

2.1 Porous silicon substrate structure

The fundamental question in metal/semiconductor junction properties, both in microelectronic and biotechnologies, is the problem of the adsorption of individual atoms on low-index surfaces silicon. Two main features are important: the configuration of adsorption sites, specific both for the roughness degree (atomic, nanometric, micrometric scale) and reconstructed (relaxed) or unreconstructed surface and the local electronic surface structure, that is the covalency or ionicity of the adsorbate-surface bond and wetting or dewetting degree. We consider the Ag atoms adhesion on relaxed dangling bond minimization surface Si (001) (2x1) with the composition and geometry shown in Fig. 1.

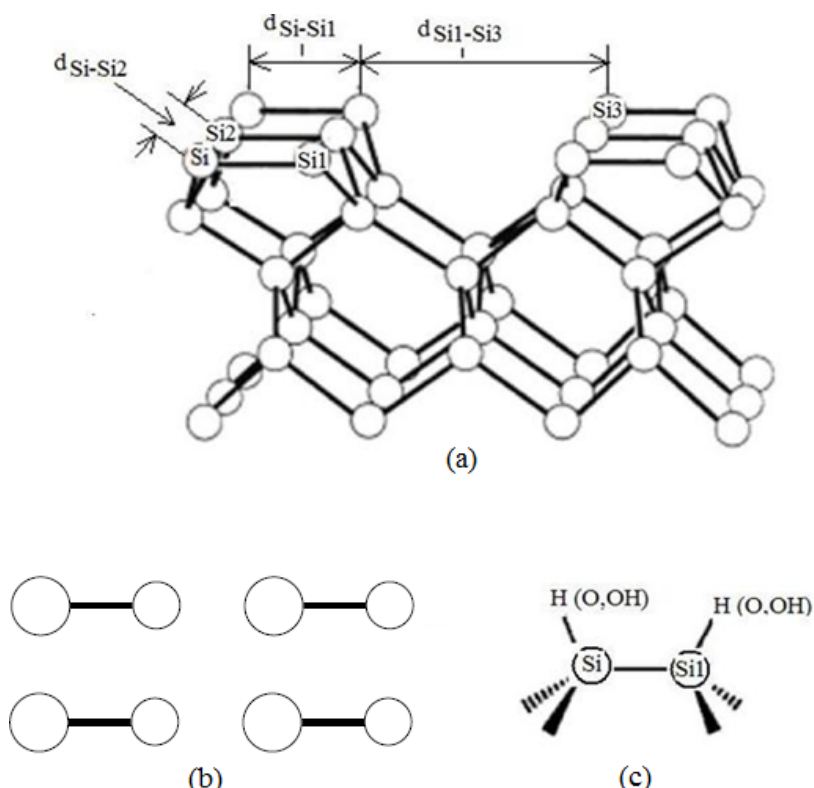


Fig. 1. Surface geometry: (a) interatomic distances on Si (001) (2x1) relaxed surface; (b) the (2x1) periodicity attributed to reconstruction based on dimer formation; (c) compensated dangling bonds on dimer (adapted from [8]).

The relaxed surface consists in any simetric dimers arrays along [110] with distance between successive

dimers on same row greater than that successive rows. Thus, each Si atom of dimer has four different-

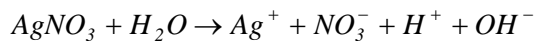
neighbours: one at $d_{Si-Si} = 2.52 \text{ \AA}$ (dimer length), two at $d_{Si-Si'} = 3.87 \text{ \AA}$ and one at $d_{Si-Si''} = 5.15 \text{ \AA}$. Each dimer surface atom have a dangling bond that may be desirable passivated. We consider three common dangling bond passivation: Si-H (H-terminated, monohydride), Si-O (oxidized) and Si-OH (hydrosilylated). Taking in account the electronegativities of the implying atoms, 1.9 for Si, 2.1 for H, 3.4 for O, [9] these bonds has different characteristics. Thus, the electronegativity difference leads to some charge transfer from a silicon atom to a hydrogen atom (hydridic hydrogen). The strong $\text{Si}^{\delta+}-\text{H}^{\delta-}$ bond is weak polar, while that for Si-O and O-H bond the electron density is skewed towards the more electronegative oxygen atom forming $\text{Si}^{\delta+}-\text{O}^{\delta-}$, $\text{O}^{\delta-}-\text{H}^{\delta+}$ polar distributions. Thus, while Si-H terminated surface has a low net dipole moment, both Si-O and Si-OH terminated surfaces have dipol moment \vec{p}_{Si-O} and $\vec{p}_{Si-OH} = \vec{p}_{Si-O} + \vec{p}_{O-H}$, respectively [10]. It is of interest to note that the polarizing effect on the Si backbonds is the same for Si-F and Si-H terminated surfaces [11].

The surface polarity due both to nanoscale surface topography and surface chemistry, plays an essential rôle on the molecular description of solvation at interfaces. The quantitative characterization of the interaction at solute/substrate interface has been show that the surface polarity rises to a substantial enhancement of surface hydrophobicity [12,13]. Thus it is possible to design of surfaces with controllable hydrophobic/hydrophilic, or more generally dewetting/wetting properties.

The H-terminated silicon surface is hydrophobic exhibiting a large contact angle for a drop af water, while the hydrophilic condition has been related to the pesence of a high superficial density of silanol groups Si-OH or to a thin interfacial oxid film. For a silanol-covered surface the contact angle depends on the relationship between Si-OH and Si-H groups, which gives rise to a dependence on solvent pH . The highest degree of hydrophobicity has been observed at solvent $pH = 11$, indicating the highest concentration of Si-H surface groups [11].

2.2 Ag/Si (001) (2x1) surface interactions

Dissociation of AgNO_3 results in Ag^+ presence in solution corresponding to reaction:



It is of interest for optical applications, to note that the NO_3^- anions presence in solution no shifts the characteristic Ag film plasma frequencies [2]. We consider separately, the Ag atoms and Ag^+ ions adhesion on PS apriori functionalized PS surface.

In modelling of the above interactions we use the pair potential consisting in a Born-Mayer term for repulsive contribution and both Coulomb long-range ionic interaction and London dispersive interaction terms as attractive contributions. For the Ag^+ adhesion at i -surface

site, the interaction energy consists in sum of ij pair atoms terms, i being Ag^+ and $j = \text{Si}, \text{H}; \text{Si}, \text{O}; \text{Si}, \text{O}, \text{H}$ atoms for Si-H, Si-O and Si-OH surface group, respectively, and can be written by:

$$V_i(r) = \sum_{j=\text{Si}, \text{H}; \text{Si}, \text{O}; \text{Si}, \text{O}, \text{H}} \left(A_{ij} e^{-b_{ij}r} + \text{erf}(b_{ij}r) \frac{q_i q_j}{4\pi\epsilon_0} \frac{1}{r_{ij}} - f_6 \frac{C_{ij}^6}{r_{ij}^6} \right)$$

where: the repulsive Born-Meyer parameters $A_{ij} = \left(A_i A_j \right)^{\frac{1}{2}}$, $b_{ij} = \frac{b_i + b_j}{2}$ are obtained from mixing rules of like-atoms pairs, $q_{i,j}$ are formal electric charges of i, j ions; the dispersion coefficients $C_{ij}^6 = \frac{3}{2} \alpha_i \alpha_j \frac{I_i I_j}{I_i + I_j}$ are obtained using the known $\alpha_{i,j}$ dipole polarizabilities and $I_{i,j}$ ionization potentials for i, j atoms; $\text{erf}(b_{ij}r)$ and $f_6 = 1 - \sum_{k=0}^6 e^{b_{ij}r_{ij}} \cdot \frac{[b_{ij}r_{ij}]^k}{k!}$ are the error function and a damping function [14] respectively, used with the role to avoid divergence of the attractive interactions at small distances.

2.2.1 Born-Mayer repulsive interactions

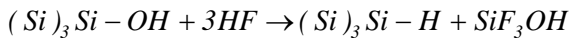
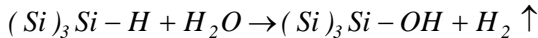
Young's modulus of hydrogen is very small, so that the $A_{\text{Ag}/\text{H}}$ and $A_{\text{Ag}^+/\text{H}}$ parameters give any negligible repulsive contributions. We consider also, the experimental fitted values $A_{\text{Ag}/\text{Si}} \cong A_{\text{Ag}^+/\text{Si}} = 1560 \text{ eV}$ and $A_{\text{Ag}/\text{O}} \cong A_{\text{Ag}^+/\text{O}} = 1128.7 \text{ eV}$ [15].

2.2.2 London dispersion interactions

1. Si-H group; The adsorption rate of atomic H and the stability of H-terminated silicon surface is due to the strong anisotropic shape of the dangling bond potential that acts as a guiding channel for the impinging H atom and prolongs the interaction time significantly. The efficiency of the H passivation of Si (001) (2 x 1) surface is assured by a sticking coefficient of atomic hydrogen $S = 0.6$ [16]. The adsorbed H atom saturates the dangling bond of the surface Si-atom so that this holds the same sp^3 hybridization as the rest of the bulk. This function is possible by modifying the properties of the hydrogen atom to siligen, that is an hydrogen atom with the 1s orbital rescaled by a suitable optimum scale factor. An estimated value of $\zeta = 0.2944$ of the scale factor of the $e^{-\zeta r}$ hydrogen Slater 1s orbital used in Si-H cluster model calculus yields an Si^{4+} ionization potential (IP) of 5.95 eV versus 5.15 eV for Si^{4+} bulk (at the valence band maximum), into an acceptable agreement with experimental values of $5.6 \div 5.9 \text{ eV}$ [17]. The pozitive

shift of $\sim 0.8\text{eV}$ of IP due to Si-H bond means higher bond energy. The same behaviour is confirmed by a positive shift of the surface Si(2p) core-level ionizations (absolute IP) from 105.39eV for bulk Si(2p) to $\sim 105.39 + 0.16\text{eV}$ for (001)(2 x 1) surface Si(2p).

2. **Si-OH group:** The Si-H terminated surface is relatively stable in air and HF etching solution, but reactive with respect to hydrolysis and Si-OH formation in an aqueous environment. The relevant reactions are (the notations refer to Fig. 1):



Concentrations ratio of hydrophobic Si-H/hydrophilic Si-OH groups on surface depends directly on alkalinity/acidity ratio of etching solution.

3. **Si-O group:** It is known that the cleaned silicon surface is not stable in air, so that quickly oxidize to form any ionic species SiO_2 hydrophilic layer. The formation hydroxyl radicals can be fast on defect sites of SiO_2 layer produced by breaking any bonds Si-O-Si. The reaction of the water with the surface strained Si-O bond can readily break forming Si-OH groups. The Si-OH is a better proton donor to the oxygen of H_2O molecule with $r(\text{Si}(\text{O}-\text{H})\dots\text{O})$ bond distances significantly shorter than $r(\text{HO}-\text{H}\dots\text{O}-\text{Si})$, so that Si-OH terminated surface has hydrophilic properties. The calculated Si-O terminated surface Si(2p) core level ionization is more positive shifted than Si-H surface, with $+1.1\text{eV}$, while the same ionization energy calculated for Si-OH terminated surface is positive shifted with $+2.8\text{eV}$ than Si-H surface [17]. The Si(2p) binding energy (BE) from XPS fumed silica measurements [18] shows an increase then the oxidation state decreases from $+4$ to $+1$. More, the average 2p BE on the central Si for Si($+1$ to $+4$) oxide and hydroxide clusters in water, are in agreement with the experimental XPS values [19] that stabilize the Si(2p) BE values, 99.8eV for Si^0 , 100.6eV for Si^{+1} , 101.6eV for Si^{2+} , 102.7eV for Si^{3+} and 103.8eV for Si^{4+} . The results are summarized in Table 1 from [18]. Thus, for Si-H/ H_2O surface, Si has $+4$ oxidation state and Si(2p) BE is $101.28 - 102.25\text{eV}$; for Si-O/ H_2O surface, Si has $+2$ oxidation state for both singlet and triplet states and Si(2p) BE is $100.53 - 101.27\text{eV}$; for Si-OH/ H_2O , Si has $+1$ oxidation state and Si(2p) BE is 100.04eV . The electronic polarizabilities associated to the different Si atom oxidation states, may be evaluated with the quantum theory relation $\alpha_s \sim \frac{\alpha_0}{E_s}$, where $s = +1, +2, +3, +4$ is the

Si oxidation state and E_s is the corresponding ionization energy. Consequently, we have been used: for Si atom, the ionization energy values $E_{+1} = 8.16\text{eV}$ for Si-OH, $E_{+2} = 16.36\text{eV}$ for Si-O and $E_{+4} = 45.196\text{eV}$ for Si-H obtained with the electronic polarizabilities $\alpha_0 = 5.4\text{\AA}^3$ and $\alpha_{+4} = 0.0165\text{\AA}^3$; for Ag atom, $E_0 = 6.886\text{eV}$ and

$\alpha_{Ag^0} = 6.33\text{\AA}^3$; for Ag^+ , $E_{+1} = 7.596\text{eV}$ and $\alpha_{Ag^+} = 0.8\text{\AA}^3$; for H^+ , $E_{+1} = 13.60\text{eV}$ and $\alpha_{H^+} = 0.15\text{\AA}^3$ [20]. For O^{2+} , E_{+2} and $\alpha_{O^{2+}}$ are from [21] and for OH^{-1} group, E_{-1} and α_{OH^-} are from [22].

2.2.3 Coulomb interactions

The long-range electrostatic interaction takes into account the formal charge (FC-electronic charge number) of the partners. The atom (or group) FC is defined by

$$FC = N_V - N_{non-bond} - \frac{1}{2}N_{bound}, \text{ where } N_V \text{ is the valence electrons number, } N_{non-bond} \text{ is the non-bonding electrons number and } N_{bound} \text{ is the total bound electrons}$$

(2 for each bond). Thus, one obtain $FC_{\text{Si}-\text{H}} = FC_{\text{Si}} + FC_{\text{H}} = 0$, $FC_{\text{Si}-\text{O}} = FC_{\text{Si}} + FC_{\text{O}} = -1$, $FC_{\text{Si}-\text{OH}} = FC_{\text{Si}} + FC_{\text{O}} + FC_{\text{H}} = -2$ and $FC_{Ag^+} = +1$

In Fig. 2 is shown the Ag^0/PS and in Fig. 3, Ag^+/PS surface interactions energy for the above three functionalized surfaces.

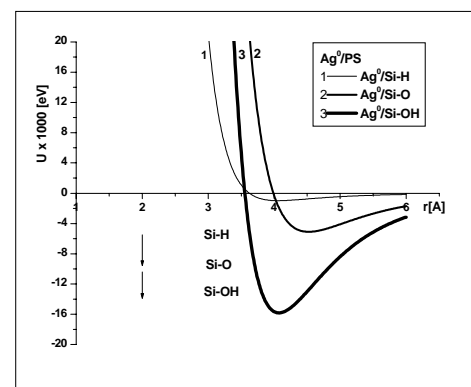


Fig. 2. $\text{Ag}^0/\text{Si-H}, \text{Si-O}, \text{Si-OH}$ functionalized PS surface interactions energy.

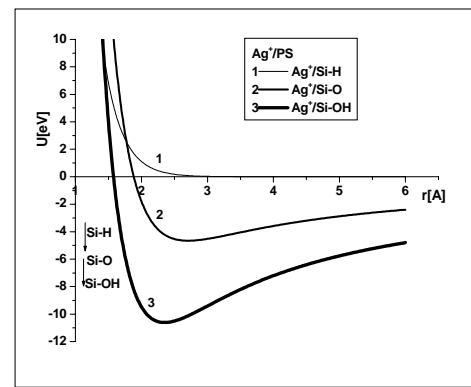


Fig. 3. $\text{Ag}^+/\text{Si-H}, \text{Si-O}, \text{Si-OH}$ functionalized PS surface interactions energy.

Obviously, the metal film stability appreciated by the binding energy metal/support, is greatest for hydrophilic

surface support (Si-O and Si-OH) for both metal atoms and ions.

2.3. Ag/Ag surface interaction

The stability of the Ag film deposited on Si substrate is assured by the equilibrium between the Ag/Si surface interactions and the Ag/Ag surface interactions. The growth process of Ag film consists in the adatom deposition, via the above interactions Ag/Si surface followed on an vertical growth by Ag/Ag specific interactions and lateral growth by specific mechanisms lateral surface diffusion. The interactions between Ag atoms may be described by a many-body potential Gupta-like [23] known as TB-SMA potential model, [24] based on the tight-binding model for transition metal cohesion in the second-moment approximation for the attractive component (the band energy of atoms system considering the covalent contributions of the d orbitals is proportional to the square root of the second-moment of the density of states) and a Born-Mayer type potential for the repulsive contributions [25].

The potential energy of atom i due to the repulsive R and attractive B interactions with neighbouring atoms, is:

$$U_i = \sum_j^n U_{ij} = \sum_j^n [U_{ij}^R(r_{ij}) + U_{ij}^B(r_{ij})] = U_i^R + U_i^B$$

where

$$U_{ij}^R(r_{ij}) = A_{ij} e^{-p_{ij}(\frac{r_{ij}}{r_0}-1)}$$

are pair-wise Born-Mayer repulsions, and

$$U_{ij}^B(r_{ij}) = \left(\zeta_{ij}^2 e^{-2q_{ij}(\frac{r_{ij}}{r_0}-1)} \right)^{\frac{1}{2}}$$

Are the n-body contributions to attractive band energy U_B^B obtained by integrating the local (total) density of states. In these expressions, n is the number of atoms within an appropriate cutoff distance r_c , so that $r_{ij} < r_c$ (we consider only the first neighbors), r_0 being the lattice nearest neighbour distance. ζ_{ij} is an effective hopping integral and q_{ij} describes its dependence on the relative interaction distance. p_{ij} describes the elastic properties of considered dimer. The range of the attractive interaction is defined by the parameter q_{ij} and the repulsive core interaction by parameter p_{ij} . At a first approximation,(for bulk) the following relations can be used for finding A_{ij} and ζ_{ij} :

$$\zeta_{ij} = \zeta = \frac{p}{p-q} \frac{E_c}{\sqrt{Z}} ; A_{ij} = A = q \frac{E_c}{(p-q)Z}$$

where p, q are the elastic bulk parameters and E_c, Z are the bulk cohesion energy and coordination number, respectively [26]. The free parameters A, ζ, p, q and r_0 are fitted to the experimental values of cohesive energy, lattice parameters (by a constraint on the atomic volume) and independent elastic constant for each system in the appropriate crystal structure and by taking the equilibrium conditions into account [24].

Bottom-up (or self-assambly) approach, as electroless deposition, to the fabrication of metallic nanostructures refers to construction of a structure atom-by-atom, molecule-by-molecule, cluster-by-cluster, placed in defined surface crystalline structure. When the size of particles is in nanometer scale, approximately all atoms are surface atoms, the nanoparticles possess a huge surface energy. The tendency to minimize the surface energy means that the many-body attractive interactions must be considered for any coordinations and bond lengths different to those of the bulk crystalline structure. Accordingly to the correlated theories of tight binding and the Local Bond Average (LDA) approximation and the Bond-Order-Length-Strength (BOLS) correlation mechanism, the spontaneous bond contraction is associated with a magnitude increase of the bond energy. The LBA approach [26] gives the performance of the local representative bonds without considering the number of bonds in the given specimen. The mathematical expression for LBA approximation is given such that any detectable quantity Q can be expressed as a function of bond identities (bond length d , bond strength E , bond nature m , and atomic coordination number Z) of the reprehensive bonds, i.e., $Q = f(d, E, m, Z)$. The BOLS correlation mechanism take into account the change of coordination number of the surface atoms and may be formulated as [28]:

$$d_i = \frac{d_B}{2} \left\{ 1 + \exp \left[\frac{12 - Z_i}{8Z_i} \right] \right\}^{-1} = d_B C_i$$

$$C_i(Z_i) = \frac{2}{1 + \exp \left[\frac{12 - Z_i}{8Z_i} \right]}$$

$$E_i = C_i(Z_i)^{-m} E_B$$

$$E_{iB} = Z_i E_i$$

where i, B denote an atom in the i -th atomic layer and in the bulk, respectively. Thus, i counts the remaining bonds between the uncoordinated atoms, with length d_i and bond energy E_i , shorther and stronger with respect to the bulk counterparts. C_i is the coefficient of bond contraction, defined as the percentage of bond length at i -th surface site to that bulk site, Z_i is the first actual coordination and m describes the nature of the bond. For pure metals of gold, copper, silver and tin, $m \approx 11$ [29]. The local bond contraction cause the potential well

depression, which enhances the overlap integral according to equations [30]:

$$\varsigma_{ij} = \langle \varphi_i | V - V_i | \varphi_j \rangle \propto E_i(Z_i)$$

where V, V_i are the crystal (bulk) and the i -th intraatomic potential, respectively; ς_{ij} is the overlap integral between i, j neighbour atomic positions.

2.3.1 A, ς , p, q considerations

We can consider that the metallic nanostructures are clusters and that the energy of atom i is given by:

$$E_i = A \sum_{j=1}^Z e^{-p(\frac{r_{ij}}{\eta}-1)} - \varsigma \sqrt{\sum_{j=1}^Z e^{-2q(\frac{r_{ij}}{\eta}-1)}}$$

Considering that in the bulk f.c.c crystal at equilibrium, $E_i = E_{coh}$, $\frac{\partial E_i}{\partial r} = 0$, at $r = r_0$, one obtain:

$$E_i = \frac{|E_{coh}|}{12(p-q)} \left[q \sum_{j=1}^Z e^{-p(\frac{r_{ij}}{\eta}-1)} - \sqrt{12} p \sqrt{\sum_{j=1}^Z e^{-2q(\frac{r_{ij}}{\eta}-1)}} \right]$$

where E_{coh} is the cohesive energy per bulk atom. The BOLS correlation considerations may be obtain, for $1 \leq Z \leq 12$ and $r_{ij} = r, \forall (ij)$ by minimization with respect to r ,

$$\frac{d(Z)}{r_0} = 1 + \frac{1}{2(p-q)} \ln \left(\frac{Z}{12} \right)$$

where $d(Z)$ is the optimum distance for Z neighbors [31]. This condition gives the difference ($p - q$) for the BOLS $d(Z_i)$ bond lengths. On the other hand, adapting the expression derived by [28], Young's modulus $Y_i = -v \frac{\partial^2 E_i}{\partial v^2} \Big|_{r=d_i}$ is proportional to the bond energy density, i.e., $Y_i \sim \frac{E_i}{d_i^3}$, and also, if we consider only the

repulsive component of $E_i, Y_i \sim p^2$. Using the bulk values p_0, q_0, r_0, E_{coh} and their values corresponding to $d(Z=1,2,3), E_{i=1,2,3} = C_{i=1,2,3}^{-1} E_{coh}$, we fit any dependences $p(d_i), q(d_i)$ from which one may obtain any desired values for the evaluation corresponding A and ς values.

The contributions to attractive band energy consist from short-ranged attractions with a steep repulsive part as

more as the hopping integral ς_{ij} increase and q_{ij} have large values, so that we may consider $\varsigma_{ij} \sim \frac{1}{d_{ij}}$ and $q_{ij} \sim \frac{1}{(r_0)_{ij}}$. On the other hand, the potential well range is a qualitative principle for the characterization of the structural features of whole atoms system, (i.e.) so that small values of q_{ij} describe soft interactions, with wide potential wells that stabilize strained structures, while large values of q_{ij} describe sticky interactions with narrow potential wells that favor crystalline structures [31].

We can suppose that a synthesis of silver nanoparticles on this surface probably will result in low-symmetry or amorphized clusters of icosahedral type by small values q_{ij} predominant interactions, and in decahedral or close-packed clusters at by high values q_{ij} . Both the distribution and concentration of the different environmental sites depend on the type of silicon relaxed surface and on the nature and intensity of the functionalized groups.

In the Table 1 we summarize the evaluated values of the parameters of TB-SMA potential used for the $\text{Ag}_{\text{adatom}}/\text{Ag}_{\text{adatom}}$ surface atoms interactions.

Table 1. Geometric and the TB-SMA potential parameters used for the $\text{Ag}_{\text{adatom}}/\text{Ag}_{\text{adatom}}$ surface atoms interactions.

Site	S1	S2	S3	S0
Distance [Å]	2.525	3.87	5.15	4.09
p	32.379	11.883		10.12
q	29.657	6.013		3.37
A	32.250	3.032		0.427
ς	35.210	4.250		1.281

The Ag/Si surface interaction results in deposition of a Ag adatom at Si-H , (or Si-O , or Si-OH) site on Si surface. A stable Ag adatom acts as a cathode, that is any others Ag^+ ions are continually reduced to neutral atoms, which are clustered around the first adatom. The vertical interaction Ag^+/Ag may be described by the above many-body potential.

2.3.2 Ag/Ag lateral surface interaction

Because the surface is a low-dimensional system, the Ag adatoms on $\text{Si}(001)(2 \times 1)$ surface occupy the under-coordinated sites ($Z < 12$) that determines the process of catalytic reactions and growth nucleation.

Assuming that the $\text{Si}(001)(2 \times 1)$ surface is uniform functionalized, each adatom site $\text{Ag}0$, named S0, has four neighbours: one, $\text{Ag}1$, at intradimer $d_1 = d_{\text{Ag-Ag}1} = d_{\text{Si-Si}} = 2.52$ Å distance and named S1; two, $\text{Ag}2$, at inter-dimer rows

$d_2 = d_{Ag-Ag2} = d_{Si-Si'} = 3.87 \text{ \AA}$ distance and named S2; one, Ag3, at dimer-dimer $d_3 = d_{Ag-Ag3} = d_{Si-Si''} = 5.15 \text{ \AA}$ distance along of the dimer row, named S3 (Fig. 4).

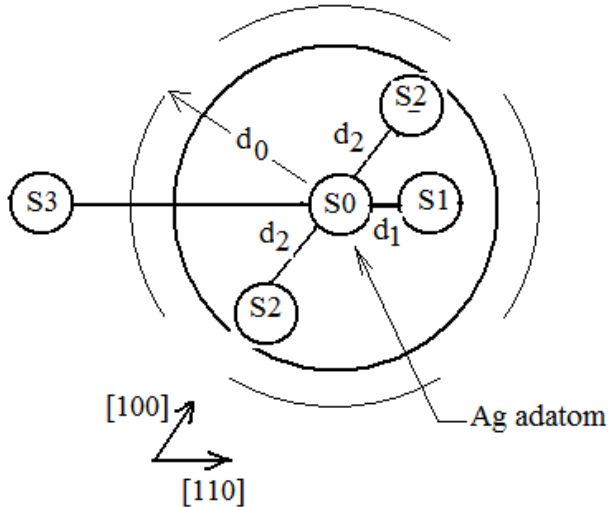


Fig. 4. Ag_{adatom} coordination.

Because the $d_1, d_2 < d_0 = 4.09 \text{ \AA}$ and $d_3 > d_0 = 4.09 \text{ \AA}$, (bulk equilibrium bond length), we consider as first neighbours only the S1, S2 adatoms. Taking into account the above considerations concerning the Ag_{adatom}/Ag_{adatom} interactions, the potential parameters from Table 1, the binding energy of an Ag adatom is $E_{adatom} = E_1(Z_1) + 2E_2(Z_2)$ and is shown in Fig. 5 by curve 2.

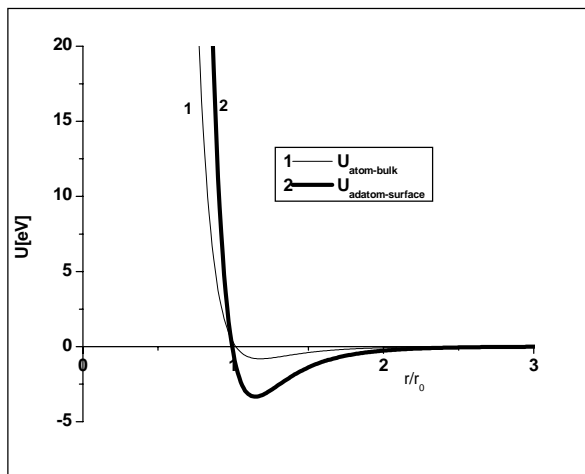


Fig. 5. Ag/Ag interaction energy: per atom-bulk (curve 1); per ad-atom (curve 2).

For S3 site, because $d_3 > d_0 = 4.09 \text{ \AA}$, the interaction $Ag0/Ag3$ is negligible so that at very low coverage are possible any breaks on the atomic layer.

Adatoms self-diffusion controls the growing process of metallic film structure and determines the surface morphology both during and after growth. At high temperature, an adatom may migrate by one of two pathways, one being the hopping mechanism, the other the exchange mechanism, correspondingly to two different dissociation mechanisms of an ad-dimer. The interaction of two adatoms is important for island formation, the adatom itself can be regarded as the smallest island. Binding energy at one surface site may be associated with the energy barrier of the ad-atom self-diffusion. Consequently, the diffusion rate and finally the island or compact film growth process are conditioned by a spatial dependence of the ad-atom/substrate interaction on a patterned surface, because $E_{diff} = E_{substrate}(x, y) + Z_i E_i$, where E_{diff} is the diffusion activation energy, $E_{substrate}(x, y)$ is the contribution due to the interaction with substrate, and E_i is the energy of interaction with other Z_i adatoms. In our model, $E_{substrate}(x, y)$ may be associated with Ag^0/PS , Ag^+/PS interaction energy, respectively and E_i with Ag_{adatom}/Ag_{adatom} interaction energy, so that the metal structures (few atomic layer thickness) deposited on hydrophilic surface consists mainly from islands, while that deposited on hydrophobic surface are rather compact films. The vertical growth is controlled by deposition method because the deposition rate is fixed from the deposition conditions.

3. Conclusions

Electroless metal deposition is an adequate method bottom-up for growth any silver thin film with the low and adaptable formation rate that favorising the coverage control. Monitoring the solution properties (pH, ionic strength) assures desirable characteristics of the functionalized support-surface (polarity, wetting, dewetting). On the other hand, the intrinsic properties of the noble metal nanostructures as thin films, are determinated by its size, morphology, composition and crystallinity. Our above analysis of the thin silver films obtained by the electroless deposition shows that this may be result in low-symmetry or amorphized clusters of icosahedral type by small values q_{ij} predominant interactions, and in decahedral or close-packed clusters for high values q_{ij} . Both the distribution and concentration of the different environmental sites of an adatom, depend on the type of silicon relaxed surface and the nature and intensity of the functionalizing groups, namely the metal film stability appreciated by the binding energy metal/support, is greatest for hydrophilic surface support ($Si-O$ and $Si-OH$) for both metal atoms and ions. Taking into account the Ag/Ag lateral surface interaction and the lateral diffusion, the metal structures (few atomic layer thickness) deposited on hydrophilic surface consists mainly from islands, while that deposited on hydrophobic surface are rather compact films.

References

- [1] J. R. Morones, J. L. Elecguerra, A. Camacho, K. Holt, J. B. Kouri, J. T. Ramirez, M. J. Yacaman, *Nanotechnology*, 2005.
- [2] X. C. Jiang, A. B. Yu, *Langmuir* **24**, 4300 (2008).
- [3] J. K. Bal, S. Hazra, *Physical Review B* **79**, 155412 (2009).
- [4] B. Gergen, H. Nienhaus, W. H. Weinberg, E. M. McFarland, *J. Vac. Sci. Technol. B* **18**(5), 2000.
- [5] Weichun Ye, Chengmin Shen, Jifa Tian, Chunming Wang, Lihong Bao, Hongjun Gao, *Electrochemistry Communication* **10**, 625 (2008).
- [6] K. J. Wan, X. F. Lin, J. Nogami, *Phys. Rev. B* **47**, 13700 (1993).
- [7] K. Sumitomo, T. Kobayashi, F. Shoji, K. Ours, I. Katayama, *Phys. Rev. Lett.* **66**, 1193 (1991).
- [8] Sun-Hee Lim, Jongbaik Ree, Yoo Hang Kim, *Bull. Korean Chem. Soc.* **20**(10), 1999.
- [9] Michael Clugston, Rosalind Flemming, *Advanced Chemistry*, University Press, Oxford, 79, (2000)
- [10] S. Romero-Vargas Castrillon, N. Giovambattista, I. A. Aksay, Pablo G. Debenedetti, *J. Phys. Chem. B* **113**, 1438 (2009)
- [11] V. Lehmann, *Electrochemistry of silicon*, Wiley-VCH Verlag GmbH.
- [12] N. Giovambattista, P. G. Debenedetti, P. J. Rossky, *PNAPS* **106**(36), 15181 (2009)
- [13] A. Ioanid, M. Dieaconu, S. Antohe, *Digest Journal of Nanomaterials and Biostructures*, Vol.5, No.4, October-December 2010, p. 947-957
- [14] T. Roussel, C. Bichara, R. J.-M. Pellenq, *NSTI-Nanotech* **3**, 660 (2005)
- [15] L. Zhigilei, *Introduction to Atomistic Simulations*, University of Virginia, MSE 4529/6270, (2008).
- [16] U. Hansen, P. Vogl, *Phys. Rev. B* **57**(20), 13295 (1998).
- [17] A. Redondo, W. A. Goddard, III, C. A. Swart, T. C. McGill, *J. Vac. Sci. Technol.* **19**(3), 498 (1981).
- [18] T.-H. Wang, J. I. Gole, M. G. White, S. C. Street, Z. Fang, D. A. Dixon, *Chemical Physics Letters* **501**, 159 (2011).
- [19] A. Hohl, H. Fuess, *J. Non-Cryst. Solids* **320**, 255 (2003).
- [20] www.Wikipedia
- [21] C. H. Hsieh, H. Jain, E. I. Kamitsos, *J. Appl. Phys.* **80**(3), 1704 (1996).
- [22] F. Torrens, G. Castellano, *10th International Electronic Conference on Synthetic Organic Chemistry (ECSOC-10)*, 1-3- November 2006.
- [23] Huan Zhan, Longjiu Cheng, Wensheng Cai, Xueguang Shao, *Chemical Physics Letters* **422**, 358 (2006).
- [24] R. F. Cleri, V. Rosato, *Phys. Rev. B* **48**(1), 22 (1993).
- [25] N. I. Papanicolaou, G. A. Evangelakis, G. C. Kallinteris, *Computational Materials Science* **10**, 105 (1998).
- [26] D. B. Graves, P. Brault, *J. Phys. D* **42**, 194011 (27pp Topical Review), 2009.
- [27] Mingxia Gu, Chang Q. Sun and Cher Ming Tan, Shanzhong wang, *Int. J. Nanotechnol.*, 2009 Interscience Enterprises Ltd. 2009.
- [28] Chang Q. Sun, H. L. Bai, B. K. Tay, S. Li, E. Y. Jiang, *J. Phys. Chem. B* **107**, 7544 (2003).
- [29] C. Q. Sun, B. K. Tay, X. T. Zeng, S. Li, T. P. Chen, J. Zhou, H. L. Bai, E. Y. Jiang, *J. Phys. Condens. Matter* **14**, 7781 (2002).
- [30] Xi Zhang, Jer-lai Kuo, Mingxia Gu, Ping Bai, Chang Q. Sun, *Graphene nanoribbon band-gap expansion: Broken-bond-induced edge strain and quantum entrapment*, www.rsc.org/nanoscale, 2010.
- [31] F. Baletto, R. Ferrando, *Rev. Of Mod Phys.* **77**, 371 (2005).

*Corresponding author: ana_ioanid@yahoo.com